Journal of
Composites Science

MDPI

Article

Processing of 3-(Trimethoxysilyl)propyl Methacrylate (TMSPM) Functionalized Barium Titanate/Photopolymer Composites: Functionalization and Process Parameter Investigation

Ajmal Zarinwall [1,†], Rytis Mitkus [2,*,†], Axel Marth [1,2], Viktor Maurer [1], Michael Sinapius [2] and Georg Garnweitner [1]

[1] Institute for Particle Technology, Technische Universität Braunschweig, Volkmaroder Strasse 5, 38104 Braunschweig, Germany
[2] Institute of Mechanics and Adaptronics, Technische Universität Braunschweig, Langer Kamp 6, 38106 Braunschweig, Germany
* Correspondence: r.mitkus@tu-braunschweig.de or mitkus.rytis@gmail.com; Tel.: +49-5313912688
† These authors contributed equally to this work.

Abstract: To improve the performance of lead-free piezoelectric composites, the functionalization of the filler particles has been suggested as a successful strategy in several recent reports. The details of the functionalization process, however, are not clear, nor is its influence on the dielectric properties of the composites. This study reports a systematic investigation of the functionalization process parameters of barium titanate nanoparticles (BTONP) with 3-(trimethoxysilyl)propyl methacrylate (TMSPM) used as a linker to an acrylate-based matrix polymer. Functionalization process temperature, time, functionalization agent ratio, solvent, and catalyst influence on the functionalization degree were measured by thermogravimetric analysis (TGA), elemental analysis, and Fourier-transform infrared (FTIR) spectroscopy. Elevated temperature and average functionalization time led to the highest functionalization degree in the form of a TMSPM monolayer on the particle surface. Three solvents, with and without catalysts, were investigated and two types of functionalized BTONP were selected for composite manufacturing. To this end, the functionalized particles were used to manufacture 10 vol.% BTONP/photopolymer UV light-curable composite suspensions. After solidification of the suspensions by exposure to UV light, the microstructure and dielectric properties of the resulting composites were investigated. It was seen that functionalization improves the dispersion of particles, increases suspension viscosity, and decreases the curing depth and dielectric properties.

Keywords: nanocomposites; surface functionalization; 3-(trimethoxysilyl)propyl methacrylate TMSPM; barium titanate; dielectric properties; photopolymerization

Citation: Zarinwall, A.; Mitkus, R.; Marth, A.; Maurer, V.; Sinapius, M.; Garnweitner, G. Processing of 3-(Trimethoxysilyl)propyl Methacrylate (TMSPM) Functionalized Barium Titanate/Photopolymer Composites: Functionalization and Process Parameter Investigation. *J. Compos. Sci.* **2023**, *7*, 47. https://doi.org/10.3390/jcs7020047

Academic Editor: Aleksander Hejna

Received: 10 November 2022
Revised: 23 December 2022
Accepted: 18 January 2023
Published: 24 January 2023

1. Introduction

Piezoelectric materials can be used in various sensing applications, such as Structural Health Monitoring (SHM), active noise control, vibration measurements, and others [1–6]. The main functional material responsible for sensor function is a piezoelectric ceramic. Because of environmental concerns and legislative restrictions, high-performance lead-based piezoelectric ceramics, such as lead zirconate titanate (PZT), need to be replaced in the near future with lower-performance lead-free piezoelectric ceramics, such as barium titanate ($BaTiO_3$ or BTO) or potassium-sodium niobate (KNN) [7]. Furthermore, researchers are actively looking for alternatives to bulk piezoelectric sensors made of pure, brittle, heavy ceramics to reduce weight, increase flexibility, and reduce the acoustic impedance mismatch between the sensors and host structures. One approach is to manufacture piezoelectric composite materials made of polymers with embedded piezoelectric ceramic nanoparticles. Such piezoelectric composite sensors offer flexibility, are simple to manufacture, and can be formed easily into various geometries [3,8–10]. However, their performance is much lower

than bulk piezoelectric ceramic sensors, and methods to increase their performance are of high interest.

Stereolithography and Digital Light Processing (DLP) 3D printing techniques have received much attention in the past decades to produce piezoelectric composites [11–19]. Stereolithography and DLP techniques both use liquid photopolymer resins as a printing material that solidifies under UV light. Photopolymer resins can be filled with piezoelectric particles to form 3D printable piezoelectric composite materials as suspensions [13,19,20]. Under UV light, these suspensions solidify and various geometries of piezoelectric sensors can be achieved [8,9,18,19]. Some studies show that specific geometries of the piezoelectric sensors can improve their performance in SHM applications [9,21]. Other studies show the possibility to obtain single-directional sensors [18,19] or to increase sensor performance in a single direction [8]. Still, the piezoelectric properties of the sensors are low and the printing process itself is complicated. Increased particle concentration is required for higher sensor performance but, at the same time, it increases the viscosity of the suspension [17,20,22] and, due to attractive particle interactions, an increased degree of particle agglomeration is observed. Furthermore, piezoelectric particles block, absorb, and scatter UV light, thus the piezoelectric composite suspensions require stronger UV light or longer exposure to solidify [12,13,17,22–26].

The low performance of piezoelectric composites comes from poor dielectric properties of the polymer which limit the maximum poling voltage, as well as poor stress transfer between polymer matrix and ceramic filler particles [19]. While the dielectric properties of the matrix can be increased by adding conductive nanomaterials [27,28], a stiffer polymer matrix can be selected to improve sensor performance [19,29]. However, the stress transfer efficiency between the polymer matrix and the ceramic nanoparticles greatly depends on particle-matrix interfacial interaction, which can be strongly influenced by a surface functionalization treatment of the filler particles. Concerning an integration of stiff piezoelectric nanoparticles in soft photopolymers, 3-(trimethoxysilyl)propyl methacrylate (TMSPM) is highly suited to be utilized as a functionalization agent due to the methacrylate groups present in both the photopolymer and TMSPM. Hence, tuning the particle surface with TMSPM provides a covalent interfacial particle-matrix linkage after embedding and polymerization that has demonstrated appreciable enhancement of the resulting composite piezoelectric properties [13,15,19]. Accordingly, the preparation of more homogeneous suspensions due to the prevention of particle agglomeration leads to improved composite processability that, in turn, facilitates an increased piezoelectric charge coefficient [13,15,19]. According to recent reports [18,19], the tailored particle-matrix interaction ensures higher strain transfer from the photopolymer to the piezoelectric particles.

Several studies have been published on piezoelectric particle functionalization for improved binding with the photopolymer matrix [13,15,19]. Escamilla-Díaz et al. [30] used TMSPM as a coupling agent to improve the compatibility between bismuth sodium titanate (BNT) and polymethyl methacrylate (PMMA). Cui et al. and Yao et al. [18,19] used TMSPM to optimize the interface between photopolymers and PZT in 3D-composite materials, whilst Gupta et al. [31] functionalized niobium-doped PZT nanoparticles with TMSPM and incorporated them into polyvinylidene fluoride-trifluoroethylene. These reports prove that TMSPM is well suited to increase the matrix-particle interaction when using piezoelectric ceramics to fill photopolymers. However, the functionalization process is time-consuming and complex. There are different possibilities for surface coordination involving one or multiple bonds [32,33]. The quality of the silane layer formation on the surface of the particles is strongly dependent on the utilized processing parameters [19].

This study aims to investigate the functionalization approach to understand the influence of the functionalization treatment on the resulting composite parameters for the further development of lead-free piezoelectric composites. The literature suggests huge improvements in functionalized particle dispersion and improved particle-matrix interface. In this work, the effect of different synthesis parameters, such as reaction temperature and time, reagent ratio, solvent variation, and the addition of acidic catalysts on the grafting

process of TMSPM onto barium titanate nanoparticles (BTONP), was thoroughly analyzed via thermogravimetric and elemental analysis. Nanocomposites filled with 10 vol.% of non-functionalized or functionalized BTONP were prepared by dispersing the particles in the photopolymer resin, followed by UV-curing. This volume percentage was selected based on our previous results [20] to achieve material compositions solidifiable under the available UV light system. The viscosities and curing depths of the prepared suspensions were measured. After composite solidification under UV light, the microstructures were investigated with scanning electron microscopy (SEM) and the influence of the functionalized particles on the resulting dielectric properties of the composites was investigated.

2. Materials and Methods

2.1. Chemicals and Reagents

BTONP (the particle size, according to manufacturer, was 100 nm, 99.99% purity) were purchased from IoLiTec Ionic Liquids Technologies GmbH (Heilbronn, Germany). 3-(Trimethoxysilyl)propyl methacrylate (TMSPM, 98%), ethanol (techn.), hydrochloric acid (37%), toluene (98.8%), acetone (≥99.5%), and isopropanol (99.5%) were supplied by Merck KGaA (Darmstadt, Germany).

The BTONP (as received from the manufacturer) were applied on conductive sticky tape and were investigated with SEM-imaging (Helios G4 CX DualBeam™, Thermo Fisher Scientific, Waltham, MA, USA). The SEM image can be found in the Supplementary Material section (Figure S1). Most BTONP are perfectly spherical; however, some particles are partially sintered together which leads to irregular-shaped aggregate particles consisting of two or more primary particles (Figure S1, red circles). Based on the SEM images, the size of BTONP was measured using the Digimizer software (MedCalc Software Ltd., Ostend, Belgium), evaluating >50 particles. Furthermore, BTONP size was also measured using Dynamic Light Scattering (DLS) (Zetasizer NANO, Malvern Panalytical, Malvern, UK). The BTONP size obtained by the Digimizer software amounted to 149 ± 46 nm, which is in agreement with DLS data, showing a particle size distribution centered at around 150 nm (Figure S2).

The commercially available "High-Temperature V2" photopolymer resin (Formlabs, Somerville, MA, USA) was used as a matrix material for piezoelectric composite manufacturing, since the literature suggests that polymers with higher stiffness can transfer more stress to ceramic particles and thus increase the overall performance of piezoelectric composites [13,19,29]. The photopolymer used here can achieve quite a high Young's modulus and high tensile strength in comparison to other commercially available photopolymers. Moreover, this photopolymer offers good temperature resistance up to 238 °C after post-curing, which is desirable for piezoelectric composites when embedding into carbon fiber-reinforced plastic structures is considered. In addition, this photopolymer has shown the best curing performance in our previous study with other ceramic particles [20].

2.2. Surface Functionalization of BTONP

The effect of various parameters on the TMSPM silanization process was examined. Before functionalization, the nanoparticles were dispersed in ethanol as a 5 wt.% suspension by ultrasonication (Bandelin UW2200, BANDELIN electronic GmbH & Co. KG, Berlin, Germany) while stirring the suspension on a magnetic stirrer plate at 670 rpm at 20 °C for 1 h. The as-prepared 5 wt.% BTONP/ethanol suspension was used for all functionalization experiments conducted in this study.

2.2.1. Investigation of Silanization Temperature

First, the influence of temperature (25 °C, 40 °C, and 75 °C) on the functionalization was investigated. The general functionalization process was performed according to Zarinwall et al. [32]. 25 mL of the 5 wt.% BTONP suspension (which equals 1.25 g_{BTONP}) was transferred into a three-necked flask and stirred at 500 rpm. Then, TMSPM was added equivalent to the mass of BTONP, which is further referred to as 100 $wt.\%_{TMSPM/BTONP}$,

and the suspension was refluxed for 24 h at 75 °C. The subsequent purification consisted of centrifugation at 19,000× *g* for 5 min, and replacing the supernatant with fresh ethanol to redisperse the BTONP using a sonication bath for 5 min at 90% intensity (SONOPLUS, mini20, BANDELIN electronic GmbH & Co. KG, Berlin, Germany). In total, this purification procedure was repeated three times to remove unbound TMSPM. Finally, the nanoparticles were dried under vacuum for 48 h at room temperature. The same purification procedure was used for all functionalized particles in this study.

2.2.2. Investigation of Silanization Time

Furthermore, the effect of the duration of the silanization treatment was studied. Functionalization was carried out as described above at 75 °C using 100 wt.% $_{TMSPM/BTONP}$. After different time intervals (ranging between 1 h and 96 h), samples were withdrawn and immediately purified to inhibit further reactions.

2.2.3. Variation of TMSPM Concentration

In addition to the silanization temperature and time, the influence of the initially added TMSPM concentration on the grafting outcome was investigated. Therefore, the added amount of TMSPM was varied from 25 to 200 wt.% in relation to the BTONP. Functionalization was performed for 24 h at 75 °C and 500 rpm as described.

2.2.4. Investigation of Acid-Catalyzed Silanization

The grafting process of organosilanes can be catalyzed by the use of acids [18]. Therefore, glacial acetic acid (AcOH) and HCl were chosen as two potential catalysts. Each substance was added in a three-fold molar excess with respect to TMSPM either to a pure ethanolic suspension (5 wt.% BTONP) or an ethanol/water mixture in a 1:1 vol% ratio (2.5 wt.% BTONP).

2.3. UV Light Curable, BTONP Filled Photopolymer Resin Preparation

Two types of TMSPM functionalized BTONP were dispersed in acetone using an ultrasonic sonotrode at 55% intensity for 15 min with 0.5 s pauses to create a 5 wt.% dispersion (pauses do not count into mixing time). Afterward, "High-Temperature V2" photopolymer resin (Formlabs, Somerville, MA, USA) is added, depending on the exact weight of BTONP used, to form a 10 vol.% BTONP/photopolymer resin combination in acetone. The mixture was sonicated with the same sonotrode at 55% intensity for 30 min with 0.2 s pauses (pauses do not count into mixing time). Then, the dispersion was put under a flue, stirred with a magnetic stirrer, and heated at 55 °C to evaporate the acetone overnight. A toothpaste-like slurry resulted, consisting of 10 vol.% functionalized BTONP nanoparticles in "High-Temperature V2" photopolymer resin. The last step before material use was degassing for approx. 4 h under vacuum at room temperature. In total, two suspensions and a reference sample with non-functionalized BTONP were prepared. The resulting suspensions had good stability at room temperature and did not show any signs of sedimentation at least for two weeks after preparation.

2.4. Composite Manufacturing

All composites in this study were manufactured by tape-casting the suspensions on the glass substrate and exposing them to UV light. A very thin mold, made of a single PVC film layer (thickness 120 µm, Oraguard 270 G, Orafol), was cut with a plotter to obtain 30 × 30 mm rectangular cut-outs and was glued on the glass. Room temperature toothpaste-like UV light curable composite suspensions were filled in the thin mold (film) glued on the glass and were tape-casted slowly with a metal blade bent at approx. 30 degrees from a vertical position. To solidify the cast suspensions, the glass with PVC film and cast materials was placed in the UV post-curing device (Form Cure, Fomlabs, USA) for 10 minutes with the heating function deactivated. 10 min were used for all suspensions prepared in this study, albeit the degree of functionalization had a clear influence on curing depth and

on mechanical properties. The post-curing device contained 13 multi-directional LEDs (wavelength 405 nm) with a total LED power of 39 W (LED radiant power is 9.1 W).

After the specimen solidification, the PVC film was peeled off keeping the manufactured composites on the glass. Then, the composites were carefully peeled off of the glass and cleaned with isopropyl alcohol. All composites were manufactured under the same conditions and had an average thickness of 120 µm. After the manufacturing, cleaning, and thickness measurements, the composites were sputtered with 28 × 28 mm size gold electrodes with a thickness of 100 nm.

2.5. Characterization

A qualitative analysis of the surface properties of BTONP was conducted via Fourier-transform infrared (FTIR) spectroscopy (data shown in the Supporting Material section). To this end, dried samples were analyzed with a Bruker Vertex 70 spectrometer (Bruker Corporation, Billerica, MA, USA) equipped with an attenuated total reflectance (ATR) cell. Quantitative information on the TMSPM functionalization was gathered using thermogravimetric (TGA) and differential thermogravimetric (DTG) analysis (1STARe system, Mettler Toledo, Columbus, OH, USA). 15 mg of dried particles were transferred into a ceramic crucible and exposed to a heating rate of 10 °C/min under an oxygen atmosphere. All results in this study are compared to a BTONP reference sample that underwent the same treatment (refluxing at 75 °C for 24 h in ethanol, drying under vacuum for 48 h) but without the addition of TMSPM. The obtained thermograms were normalized at 150 °C to exclude the effect of varying amounts of physisorbed solvent and water of the individual samples. Finally, the absolute mass losses were determined at 850 °C. The measurement inaccuracy was determined to be ± 0.08 wt.% by measuring the 100 wt.% $_{\text{TMSPM/BTONP}}$ sample three times. In addition, elemental analysis (EA) of silanized BTONP was conducted with a FlashEA 1112 from Thermo Quest (Waltham, MA, USA) for validating the obtained TGA results. Based on the difference in the determined carbon content from modified ($C\%_{\text{modified}}$) and unmodified ($C\%_{unmodified}$) BTONP, the molar concentration of bound TMPSPM (c_{TMSPM}) per g_{BTONP} was calculated according to Equation (1):

$$c_{TMSPM} = \frac{\left((C\%_{\text{modified}} - C\%_{unmodified}\right)/100)}{n_C \times \mathrm{M}_C} \text{ given in } mol_{TMSPM} \times g_{BTONP}^{-1} \quad (1)$$

with M_C and n_C being the atomic mass (12 g/mol) and the number of carbon atoms, respectively. Assuming the formation of a homogenous monolayer as a result of complete TMSPM hydrolysis, solely the mass of the carbon atoms of the propyl methacrylate (PMA) group (n_C = 7) needs to be considered. The number of molecules grafted on the BTONP surface per square nanometer (referred to as grafting density δ_{TMSPM}) was finally calculated as:

$$\delta_{TMSPM} = \frac{c_{TMSPM} \times N_A}{S_A \times 10^{18}} \text{ given in } molecules \times \mathrm{nm}^{-2} \quad (2)$$

where N_A is the Avogadro number (6.02 × 10^{23} mol^{-1}) and S_A represents the specific surface area in m^2 g^{-1}. S_A was determined via nitrogen sorption analysis using a multi-point Brunauer–Emmett–Teller (BET) surface analyzer (ASAP 2460, Micromeritics GmbH, Unterschleissheim, Germany).

Energy-dispersive X-ray spectroscopy (EDX) characterization was made with the EDAX Octane Elite-70 of AMETEK Materials Analysis Division (Mahwah, NJ, USA).

The viscosities of the BTONP-filled photopolymer resins prepared in this study were measured with a rheometer (Anton Paar MCR 702, Anton Paar Germany GmbH, Ostfildern-Scharnhausen, Germany) over varying the shear rate from 1 to 30 s^{-1} at room temperature (25 °C). A varying shear rate was selected based on our previous studies where a clear shear-thinning effect was observed [20]. The metal plates measuring the viscosity had a diameter of 25 mm and the distance between the plates was set to 1 mm.

The curing depths of the suspensions were measured over time, using four curing times: 10, 20, 30, and 40 min. The specially designed, pre-cut PVC film (Oracal 751C, black matt, thickness 60 µm) with cut holes was glued onto the glass plate [34]. For every curing time and material composition, 5 to 6 holes were used to measure the average curing depth. The film was designed in such a way that specific holes can be covered with a cardboard mask, creating different exposure times for specific holes. Below the glass, a 1-mm-deep container was filled with the suspension to measure its curing depth, and the glass with a PVC film was placed on top, leaving no air bubbles trapped. The setup was covered from all sides except the top surface to protect it from the UV light coming from the bottom or other sides. This whole setup was transferred to a post-curing UV device (the same as used for manufacturing) to cure for the first 10 min. The heating function was deactivated. After the first 10 min, the first cardboard mask (covering 5 holes) was placed on the respective holes to block UV light from further curing and the whole setup was cured for the next 10 min. Another mask was added, covering additional holes, and the process was repeated until the final curing time (40 min) for the last holes was reached. The container with the suspensions was removed and the solidified composite material on the glass was cleaned with isopropyl alcohol. The height of the cured circles (5 to 6 cured circles per curing time for every suspension) was measured with a laser distance sensor. The curing depth measurement technique and the procedure are described in our previous publications [20,34,35].

Relative permittivity at different frequencies was calculated from Eq. 3 after measuring the capacitance of the solidified composites at room temperature at frequencies of 100 Hz–100 kHz. Two gold electrodes were sputtered with a thickness of 100 nm on both sides of the composites. Capacitance was measured with an LCR meter (Voltcraft LCR-300, Conrad Electronic SE, Hirschau, Germany, accuracy of 0.3% with 0.01 digit resolution). The electrode area was calculated from manual measurements with a ruler with 0.5 mm accuracy. The dissipation factor was measured directly with the same LCR-300 meter.

$$\varepsilon_r = \frac{C \times d}{\varepsilon_0 \times A} \tag{3}$$

where C—capacitance of the sensor at a frequency of interest (F), d—average thickness of the sensor (m), ε_0—vacuum permittivity, constant (8.84 $\times$ 10^{-12} F/m), A—overlapping electrode area of the sensor (m^2).

3. Results and Discussion

This study aimed to systematically analyze the TMSPM silanization of BTONP and consequently elucidate the influence of tuned surface properties on the subsequent curing process and the resulting dielectric properties of the manufactured composites. Therefore, an in-depth characterization of the functionalized BTONP, the UV light curable ceramic/photopolymer suspensions, and finally, the solidified composites was carried out.

3.1. Particle Functionalization—Influence of TMSPM/BTONP Ratio

The influence of the used TMSPM concentration on the resulting degree of functionalization was examined by TGA and DTG (Figure 1A,B).

The mass loss events in the obtained thermograms of plain and functionalized BTONP below 150 °C (see Figure S3) can be assigned to the desorption of physically adsorbed solvent molecules [36]. Since the precise quantity of physisorbed molecules varied between the different samples, a normalization of the TGA and DTG curves was performed at 150 °C (Figure 1A,B). Upon further heating of BTONP, dehydroxylation of the BTONP surface and decomposition of synthesis-related residual organics, as well as the presence of barium carbonate, lead to a total mass loss of approximately 3.9 wt.% [37]. The TGA/DTG results of all TMSPM-functionalized BTONP samples display similar profiles that mainly differ by the extent of mass loss due to different degrees of functionalization. To determine the specific mass loss related to the attached TMSPM on the BTONP surface, values at

850 °C were chosen for the quantification. Therefore, the obtained data were plotted as a function of the initially added amount of TMSPM with respect to the mass of BTONP in the suspension (Figure 2).

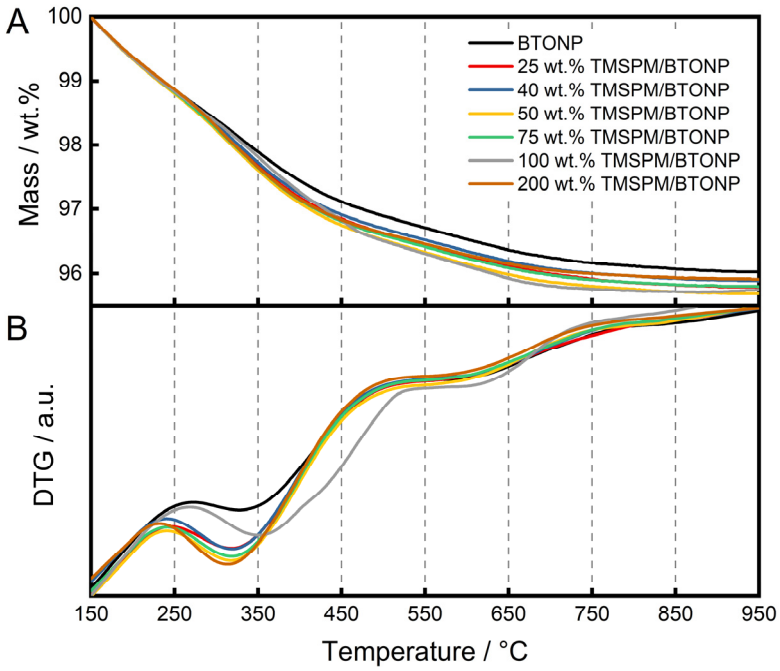

Figure 1. (**A**) TGA profiles of BTONP before and after functionalization with different amounts of TMSPM, normalized to 150 °C. (**B**) Respective DTG profiles.

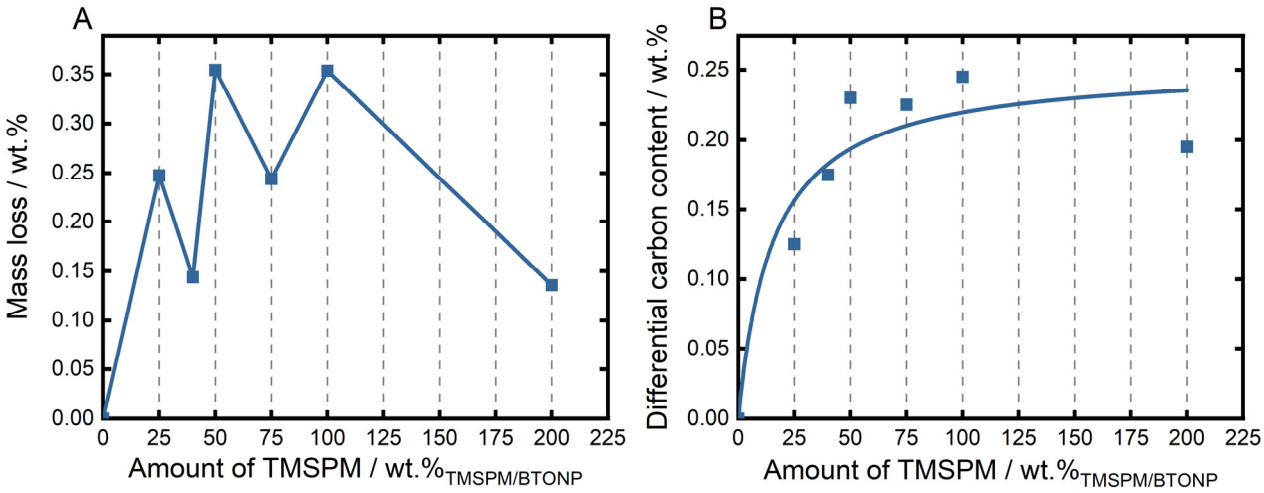

Figure 2. (**A**) TMSPM-related mass loss (TGA) and (**B**) carbon content as a function of the initially added amount of TMSPM.

Notably, only a small increase in mass loss was observed after functionalization and no distinct trend was obtained from the TGA-derived data (Figure 2A). Due to the system-related error susceptibility of ±0.08 wt.% and the relatively small differences in the obtained mass losses, a reliable data evaluation by TGA was not feasible. However, a roughly converging behavior can be approximated. Hence, the carbon content of the differently prepared sample fractions was additionally determined using EA to validate the amount of TMSPM grafted to the BTONP surface. The recorded carbon content of the reference sample (0.09 wt.% $_{TMSPM}$) was subtracted from the modified samples, and thus a differential carbon content is displayed. With up to a ratio of 50 wt.%$_{TMSPM}$, a steady

increase in the recorded carbon content was obtained that can be correlated with the quantitative coordination of the added TMSPM on the BTONP (see below). Thereafter, a more consistent converging behavior was attained compared to the TGA-based quantification. Consequently, the gathered experimental data were fitted via the Langmuir adsorption model, which describes the monomolecular adsorption of the adsorbate to equivalent surface sites. Although the Langmuir model furthermore assumes that there are no interactions between the adsorbed molecules, it is widely used to describe the organosilane-based monolayer growth [32,38–40]. Since the carbon contents for larger amounts of added TMSPM remained almost constant, a complete occupation of all accessible surface OH-sites on the BTONP can be assumed. The relatively small determined grafted quantities, however, result from the rather low specific surface area, which was determined to be 10.5 m^2/g utilizing nitrogen sorption analysis. Thus, using Equations (1) and (2), a grafting density of 1.5 molecules $_{TMSPM}/nm^2$ was ascertained for concentrations above 50 wt.% $_{TMSPM}$. According to our previous studies [32,41,42], this evidences the formation of a homogenous and stable TMSPM monolayer on the particle surface, since grafting densities ranging from 1.1 to 2.0 molecules/nm^2 of different silanes on various particle systems are classified to be characteristic for monolayer formation [43–45].

In addition to the quantitative characterization, qualitative proof of the successful TMSPM attachment on the particle surface was obtained via FTIR measurements (Figure 3).

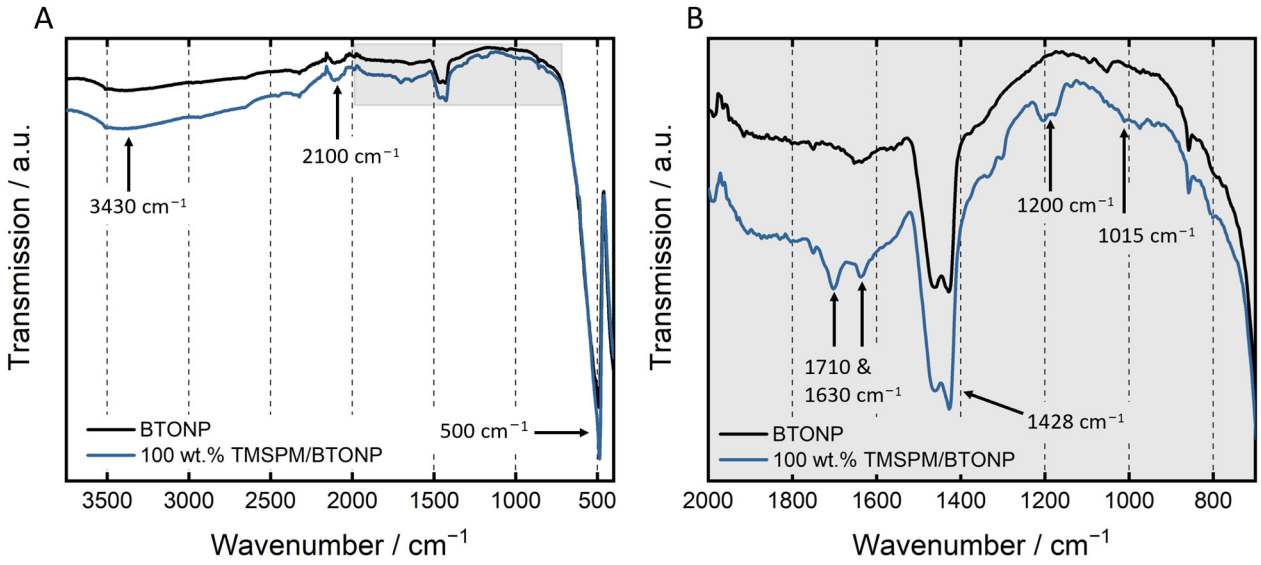

Figure 3. (**A**) FTIR spectra of plain and TMSPM-functionalized BTONP that were processed in ethanol at 75 °C for 24 h with a weight ratio of 100 wt% $_{TMSPM/BTONP}$. (**B**) Magnified grey area in the wavenumber range between 2000 and 700 cm^{-1} for better visibility of the relevant signals.

The FTIR spectrum of plain BTONP (Figure 3A,B) shows a broad absorption band centered at 3430 cm^{-1}, which corresponds to the stretching mode of O–H groups, e.g., of adsorbed water and surface hydroxyl groups [46]. The broad signal at 2100 cm^{-1} is due to CO_2 within the measurement chamber and, thus, does not represent a sample-specific signal. The characteristic signal at around 500 cm^{-1} can be ascribed to the Ti–O vibration mode of $BaTiO_3$ and confirms its crystalline state [47,48]. Furthermore, the peak at 1428 cm^{-1} can be attributed to the C–O stretching vibration in CO_3^{2-} presumably present as synthesis-related residual traces of barium carbonate ($BaCO_3$) [49]. The TMSPM-functionalized BTONP additionally exhibited two bands at 1710 and 1630 cm^{-1}, which can be assigned to the stretching vibration of the alkene (C=C) and the carbonyl (C=O) groups, respectively. Moreover, a signal at 1200 cm^{-1} is apparent that arose due to the C–O–C skeletal vibration originating from the methacrylate group [50]. Due to the formation of a monolayered polysiloxane network, the corresponding signal for the asymmetric stretching vibration of Si-O-Si at 1015 cm^{-1} appeared only at low intensity. Nevertheless, these

findings validate and further confirm the successful binding of TMSPM to the particle surface [15,18,51].

3.2. TMSPM Functionalization—Influence of Temperature, Time, and pH

To establish an efficient and cost-effective functionalization process, the significance of the temperature and reaction time was examined and their influence on the resulting grafting densities was determined (Figure 4 and Supplementary Material Figures S4 and S5).

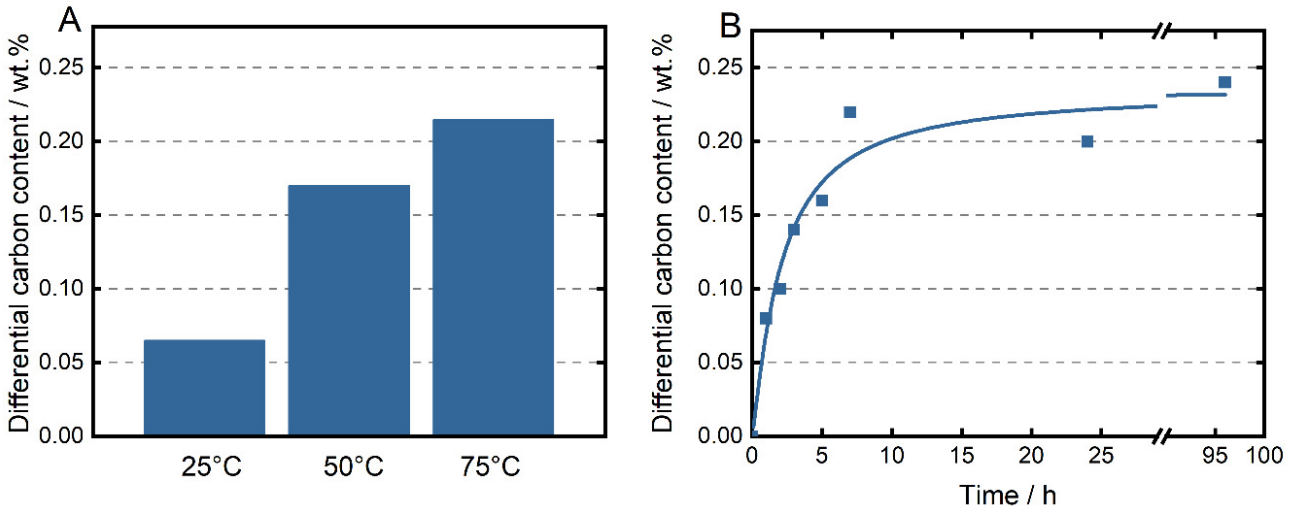

Figure 4. Carbon content of TMSPM-functionalized BTONP (100 wt.% $_{TMSPM/BTONP}$) determined via elemental analysis for functionalization carried out (**A**) at different reaction temperatures for 7 h and (**B**) for different reaction times at 75 °C.

The amount of attached TMSPM on the particle surface was quantified via elemental analysis, yielding the relative weight percentage of carbon in the sample as described above. As can be deduced from Figure 4A, the grafting efficiency was decisively enhanced at elevated temperatures (75 °C). Accordingly, functionalization at room temperature (25 °C) did not result in any significant changes in the determined carbon content while an increase of 0.17 and 0.22 wt.% was recorded for grafting at 50 °C and 75 °C, respectively. At these elevated temperatures, the miscibility of the constituents is remarkably affected [52], the Brownian motion is accelerated, and the reaction rate increases, which, in total, facilitates the particle-ligand interaction and hence promotes the coordination of TMSPM, leading to an increased quantity of attached linker molecules [32,49,50,53–55]. In addition to the temperature, silanization was further shown to be a function of time with the reaction kinetics following again the Langmuir model [38,40,56]. Accordingly, monolayer formation took place within the first 7 h, reaching a plateau at 0.22 wt.% carbon content. As longer functionalization times do not seem to facilitate a further increase in the grafting amount, the treatment at 75 °C for 7 h is identified as optimal. However, regarding the subsequent embedding of the BTONP in the polymer matrix, an increased functionalization density could be highly beneficial because of improved particle-matrix compatibility and enhanced interfacial interactions.

In general, it is well known that the addition of water and acidic catalysts exerts a considerable influence on the hydrolysis reaction of alkoxysilanes and, thus, on the functionalization density since the reactivity of the hydrolyzed silane molecules becomes substantially enhanced [57]. Hence, the use of catalysts was investigated in the TMSPM silanization process of BTONP.

It is well known that the hydrolysis rate of silicon alkoxides is lowest at a neutral pH and that it rises with increasing concentrations of protons [57]. Hence, surface functionalization by TMSPM is often carried out using acetic acid (AcOH) as a catalyst [13,15,18]. As obtained from elemental analysis, however, the sole addition of AcOH to an ethanolic

suspension of BTONP was not sufficient to increase the grafting density but showed slightly decreased carbon contents, which is attributed to measurement inaccuracies (Figure 5). When additional water was supplied to the EtOH/AcOH mixture (EtOH/H_2O/AcOH), only a small increase in the determined carbon content was observed. However, when HCl was applied as a catalyst (EtOH/H_2O/HCl), the catalytic efficiency was substantially enhanced, resulting in a significant increase in the determined carbon content (0.78 wt.%). The presence of water accelerates the rate of hydrolysis that, in turn, leads to enhanced reactivity. In addition, under acidic conditions, the alkoxy oxygens of TMSPM become protonated and are then substituted by a nucleophilic attack of water, resulting in more reactive Si-OH monomers and, thus, in an enlarged magnitude of TMSPM crosslinking [32,57,58]. Consequently, a grafting density of 5.2 molecules $_{TMSPM}/nm^2$ was calculated, indicating that TMSPM not only forms a monolayer on the BTONP surface but also condenses into structures that partially extend vertically from the surface. The stronger influence of HCl on the catalysis efficiency in contrast to AcOH can be attributed to its much higher acidity ($pKa_{HCl} = -7$) compared to AcOH ($pKa_{AcOH} = 4.8$) [59,60]. Thus, the functionalization treatment in an aqueous acid solution promotes the surface coverage noticeably. Hence, depending on the chosen process parameters, different coordination modes, i.e., a monolayer (EtOH) or polylayer arrangement (EtOH/H_2O/HCl) of TMSPM on the particle surface was achieved. The influence of the resulting different amounts of bound TMSPM on the subsequent processing of the nanocomposites is discussed in the following sections.

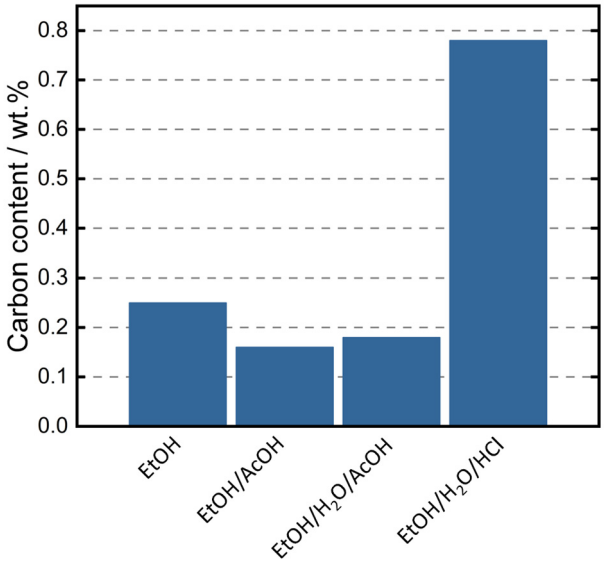

Figure 5. Carbon content of BTONP after TMSPM functionalization treatment using different solvent compositions with the addition of water, glacial acetic acid, and hydrochloric acid.

3.3. Viscosity and Curing Depth

The viscosity of the photopolymer resin after embedment of the functionalized BTONP was measured to understand how particle functionalization influences the rheological properties. Additionally, the curing depth was investigated to clarify the influence of functionalization on composite manufacturability. Both parameters are important for the printability of the suspensions. Details of the suspension preparation can be found in the Supplementary Material. Viscosity that is too high makes the suspensions unusable with commercially available SLA/DLP type 3D printers and—as the viscosity is known to increase drastically with the particle content—limits the maximum possible ceramic loading. Furthermore, a reduction in curing depth increases the required UV light dosage to solidify a composite, creates over-exposure of surface layers, and renders the composite solidification process more complex.

At low shear rates, the viscosity of the resins with functionalized particles is higher than the sample without functionalization (BTONP, see Figure 6A), while at higher shear rates, the viscosity is lower. The increase in viscosity of the suspensions with functionalized particles can be linked to the decreased particle size due to less agglomeration in the photopolymer, which is observed in SEM images (Figure 7). It is generally known that smaller particles or smaller agglomerates lead to a higher increase in suspension viscosity. However, since the SEM images prove that the composites show a significantly reduced agglomeration tendency in comparison with the BTONP reference sample already after standard functionalization in EtOH, a higher functionalization degree might not increase viscosity further. Additionally, for the higher degree of functionalization (after treatment in EtOH/H_2O/HCl), TMSPM was identified to extend vertically from the particle surface, as discussed above. This might reduce particle interactions as a result of steric stabilization and thus provides lower viscosity. Decreased viscosity at higher shear rates is beneficial and faster tape casting speeds or faster layer recoating motions (in 3D printers) can be used to achieve higher-quality specimens.

The resins filled with functionalized particles show lower curing depths in comparison to the non-functionalized sample (BTONP, Figure 6B). These results can be explained by a more even distribution of functionalized BTONP and the formation of fewer agglomerates, hence a lower (secondary) particle size. The literature reports that composites filled with smaller ceramic particles produce lower curing depths [17,23,25] because the ceramic particles physically block UV light from penetrating deeper and scatter it to the sides. Therefore, instead of increasing the curing depth, the width of the curing increases but the depth of curing decreases. Due to its higher inhomogeneity, the reference sample (BTONP, Figure 6B) shows a higher standard deviation compared to the samples containing functionalized particles. The composite containing particles with the highest degree of functionalization (EtOH/H_2O/HCl) displays the lowest curing depth and smallest standard deviation, thus indicating an elevated degree of homogeneity originating from an improved particle-matrix interaction by functionalization.

The measurements of viscosity and curing depth hence confirm that, through the functionalization treatment, smaller agglomerates are achieved, due to the higher stability of functionalized particles within the photopolymer and due to the interaction of the methacrylate groups of the TMSPM with the photopolymer. The observed increase in viscosity at low shear rates and reduction in curing depth are not favorable for a UV light-curable material; however, improved homogeneity and improved particle-matrix interaction counterweigh these disadvantages.

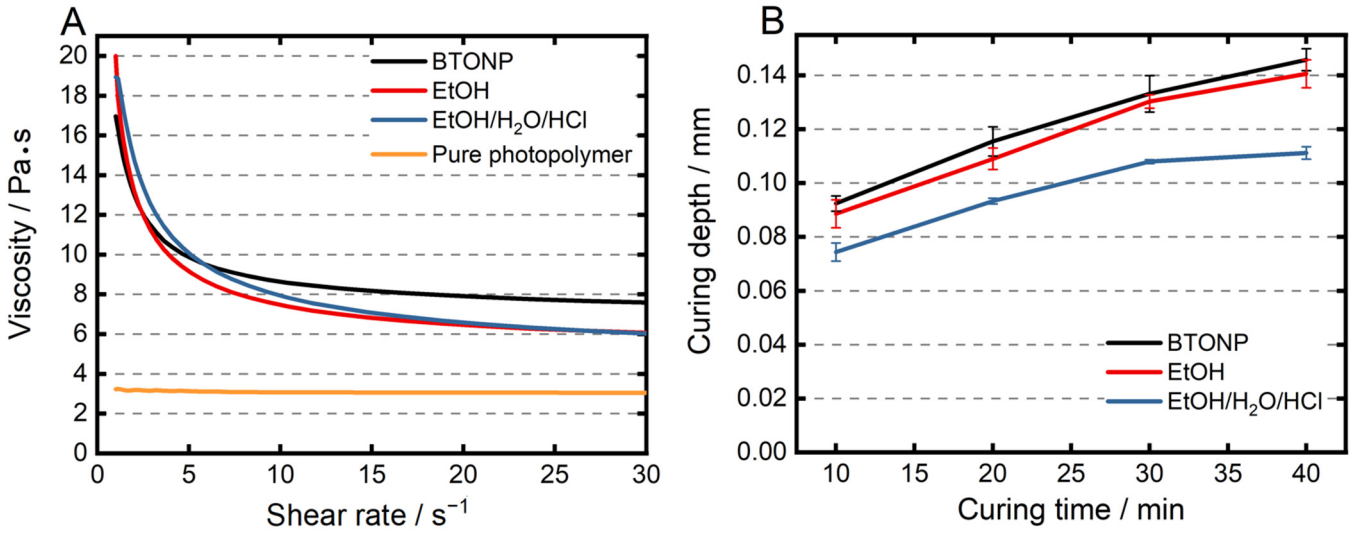

Figure 6. Characterization of photopolymer resins containing 10 vol.% of functionalized BTONP at room temperature; (**A**) Viscosity over shear rate; (**B**) Curing depth over time.

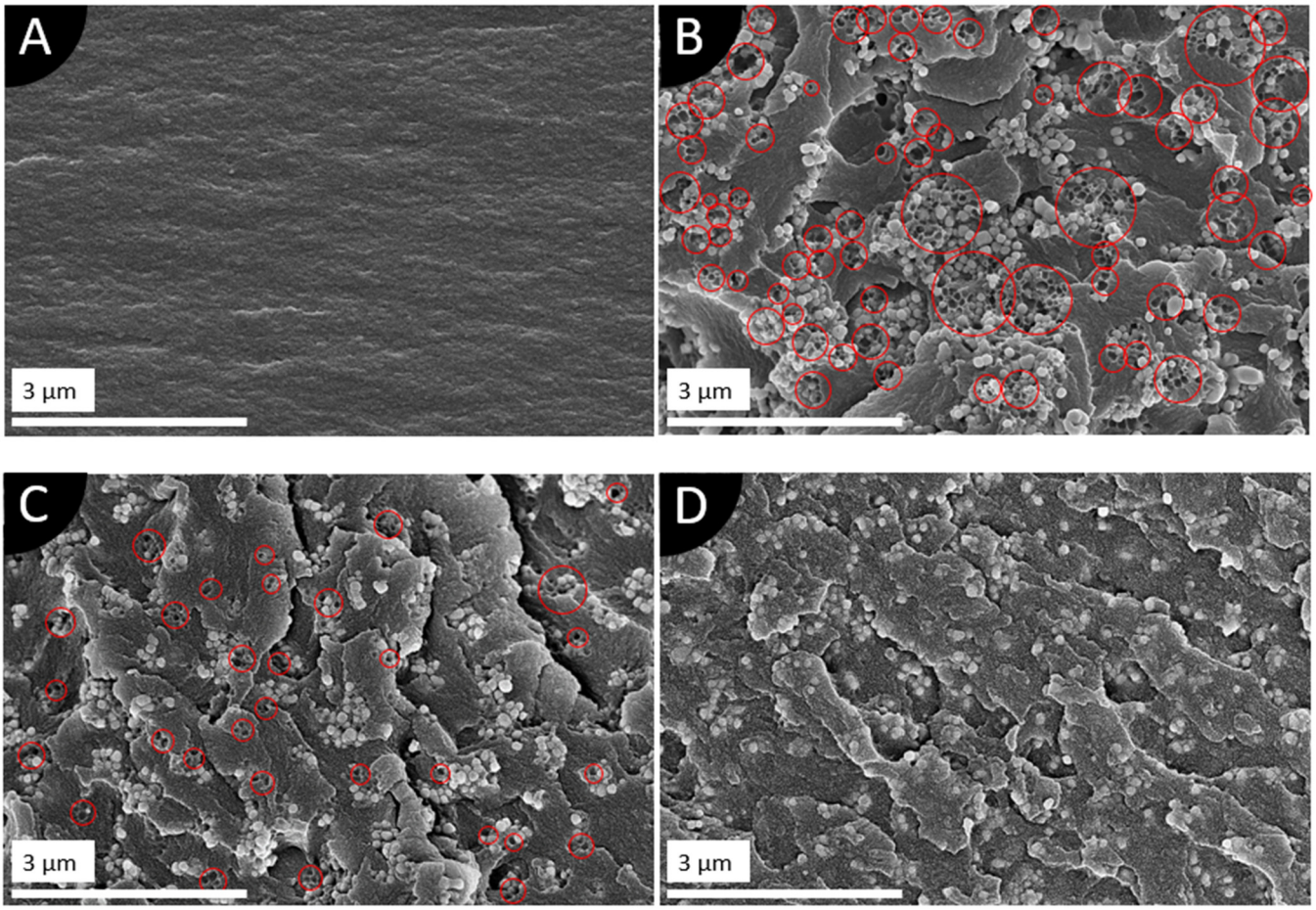

Figure 7. SEM images of composites after fracturing at room temperature. All composites contain 10 vol.% of: (**A**) Bare photopolymer; (**B**) Non-functionalized BTONP; (**C**) Functionalized BTONP (EtOH); (**D**) Functionalized BTONP (EtOH/H_2O/HCl). Red circles indicate missing particles.

3.4. Microstructure of the Composites

Solid composites were manufactured from the prepared suspensions to analyze their microstructure and measure their dielectric properties. The solidification procedure was kept the same for all composites and is described in detail in the Supplementary Material. All composites were solidified under UV light. Therefore, taking into account reduced curing depth while using functionalized particles (Figure 6B), a slightly lower curing degree of the photopolymer can be expected which, however, should not have any significant influence on the microstructure.

The solidified composites were broken at room temperature to investigate their cross-sections and to determine the particle distribution. The obtained SEM micrographs of the composites are shown in Figure 7 at a magnification of ×50,000. Red circles in Figure 7 show locations of missing particles that detached during composite breaking, indicating poor particle-matrix adhesion. The same images as in Figure 7, but without red circles, can be found in the Supplementary Material (Figure S6) together with additional SEM images at ×20,000 (Figure S7).

In contrast to the smooth microstructure of the bare photopolymer as reference (Figure 7A), the filler particles are clearly visible in all composites. The sample made with BTONP, as received from the manufacturer (Figure 7B), appears to contain a higher number of ceramic particles compared to the composites with functionalized particles according to the images in Figure 7C,D. However, the surface of the composite cross-section (Figure 7B) seems to be very rough, revealing more particles. Moreover, half of the circular shapes in the SEM image (Figure 7B) do not display particles but rather the cavities left after the breaking of

the composite, indicating poor interfacial adhesion between the ceramic particles and the photopolymer matrix. Furthermore, a tendency to form agglomerates is visible.

The microstructure of the composites with functionalized particles shows a clear improvement in particle dispersion, particle distribution, and interfacial adhesion between the particles and the polymer matrix with an increasing degree of particle functionalization. A smaller number of agglomerates is present in comparison to the sample with non-functionalized BTONP (Figure 7B). Yet, smaller agglomerates of a few particles each are formed in the composite with BTONP functionalized with TMSPM in a monolayered order (Figure 7C). To ensure that the functionalized and non-functionalized BTONPs were not dispersed into the resin in an agglomerated state, the hydrodynamic diameter of BTONP in ethanol was determined with DLS before and after functionalization (Figure S2), proving that no agglomeration occurred during functionalization. Therefore, the small agglomerates visible in the SEM images were most probably formed after the surface modification while dispersing functionalized BTONP into the resin. The particle distribution in the resin is best for the particles with the highest functionalization degree (Figure 7D).

Moreover, the composites containing BTONP functionalized in EtOH show fewer voids due to missing particles compared to the sample with non-functionalized BTONP. It needs to be stated that the shape of the cavities seems to be very similar between both composites, but the cavities in the composite with non-functionalized BTONP extend much deeper into the matrix network (Figure 7B and Supplementary Material Figure S6A) compared to those resulting from the BTONP functionalized in EtOH (Figure 7C and Supplementary Material Figure S6B). Moreover, the density of cavities is highest for the plain BTONP, followed by TMSPM-functionalized particles in EtOH, whereas the composite with BTONP having polylayered TMSPM bound on the particle surface does not exhibit any cavities at all. This can be ascribed to the improved chemical compatibility of the TMSPM-functionalized BTONP with the matrix, resulting in a higher and more homogenous polymer network density in the interphase and, thus, in improved particle-matrix adhesion. In contrast, hydroxyl-terminated plain BTONP are not capable of cross-linking with the matrix, which presumably leads to less homogenous interphase, and thus a poor particle-matrix adhesion. Furthermore, the sample with particles functionalized in EtOH/H_2O/HCl exhibits the smoothest cross-section, possibly due to slightly lower mechanical properties of the matrix (lower stiffness) that result from the highest reduction of the curing depth for this composite.

The SEM images suggest that functionalization indeed improves particle dispersion, helps to maintain a homogeneous distribution of the ceramic particles in the photopolymer resin during composite material preparation and manufacturing, and enhances the particle-matrix interface adhesion. It is also clear that the degree of particle functionalization plays a key role in improving particle dispersion and particle-matrix interface adhesion, since composites with multilayer-functionalized BTONP (EtOH/H_2O/HCl) showed the best homogeneity and highest interfacial adhesion. A similar improvement of particle dispersion when using silane-functionalized BTO particles has been reported in the literature [36,61].

3.5. Dielectric Properties

The dielectric constant (relative permittivity) ε_r and dielectric loss (dissipation factor, tan δ) were measured at room temperature to investigate the influence of particle functionalization on the dielectric properties of the resulting composites. Low relative permittivity increases the electrical output of the piezoelectric material, which is beneficial for sensing and energy-harvesting applications [2]. However, lower relative permittivity leads to a decrease in polarization efficiency because of a reduction in breakdown voltage [62]. Ideally, composites should have a dielectric constant as high as possible and dielectric loss as low as possible during poling, while possessing a homogeneous particle distribution, but low dielectric constant and low dielectric losses after poling for the highest performance. Our previous results suggested exactly this behavior of the photopolymer used in this study, with high dielectric constants being achievable with an average curing degree of the pho-

topolymer, and a decrease in dielectric constant resulting upon further curing [34]. Many studies reported increased dielectric properties of composites filled with functionalized BTO particles when using various silane-based functionalization agents [36,61,63,64].

Figure 8A shows the dielectric constant and Figure 8B presents the dielectric loss of all composites manufactured in this study. The dielectric properties of the pure photopolymer are also added for comparison. As can be seen, the addition of 10 vol.% of BTONP (both functionalized and non-functionalized) to the photopolymer increases the dielectric constant.

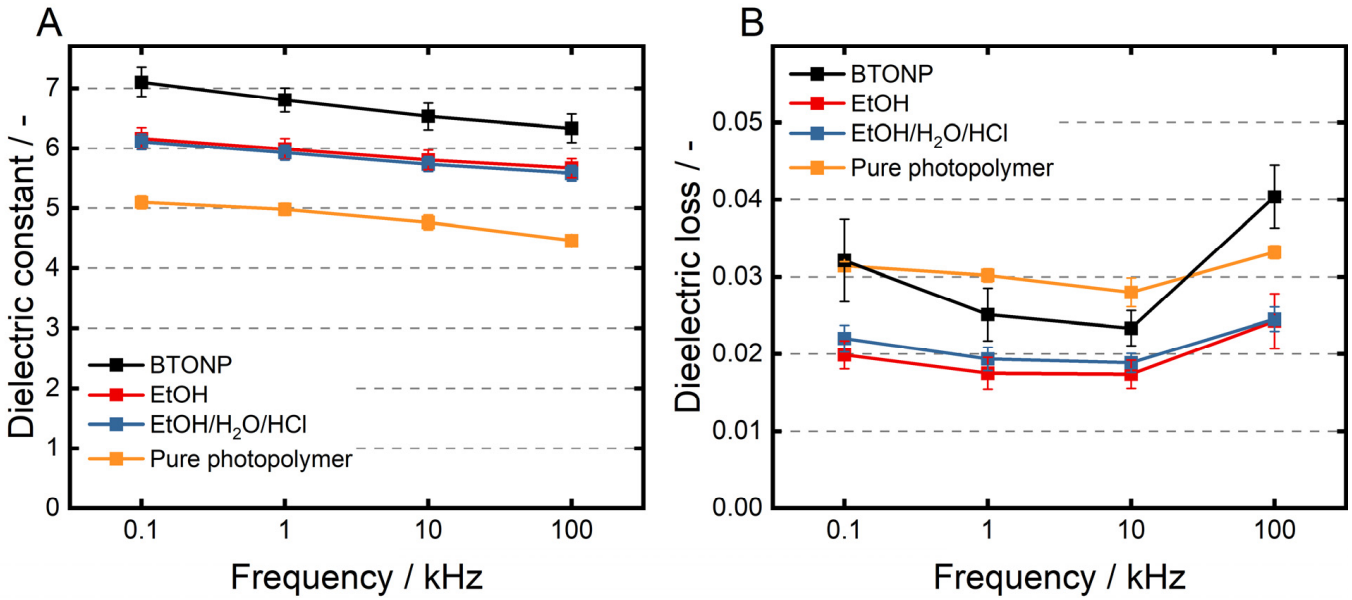

Figure 8. Dielectric properties at room temperature of composites made of photopolymer resin filled with 10 vol.% non-functionalized and functionalized BTONP: (**A**) Dielectric constant (relative permittivity); (**B**) Dielectric loss (dissipation factor). The straight lines connecting the data points at different frequencies do not represent linear trends and only connect points for visual purposes.

Non-functionalized particles produce an increase in dielectric constant that is almost twice as high as that of functionalized particles. To be precise, the functionalization increased the dielectric constant at 1 kHz by approx. 19%, while the non-functionalized particles led to an increase by approx. 36%. The dielectric constant decreases with frequency as expected, while dielectric losses decrease up to 10 kHz and start to increase again. Decreasing dielectric constant with an increasing frequency has been reported for piezoelectric composites in other works [65].

Dielectric losses decrease with particle functionalization, which is highly desirable. Non-functionalized BTONP show increased dielectric losses at higher frequencies. A similar rising trend of the dielectric losses of composites with functionalized BTO particles at frequencies higher than 10 kHz is reported in the literature [36].

Interestingly, all composites made with functionalized particles show quite similar dielectric constants which almost fit within the standard deviation, suggesting no or very small difference. The decrease in dielectric constant compared to the non-functionalized BTONP reference can be attributed to improved particle dispersion. As explained by Robertson et al. [66], agglomerated particles present lower impedance for an electric flux between electrodes because of the higher number of particles in a line perpendicular to the electrodes. If a good dispersion of the particles is achieved, the particle-matrix ratio in that specific volume section is lower, and more of the polymer is in the path of electric flux lines. This causes higher electric impedance and, as a result, lower relative permittivity.

The higher interface area between the functionalized BTONP and the composite matrix (due to better particle dispersion) also contributes to lower dielectric properties. In cement matrices with non-functionalized PZT particles, this increase in surface area, because of better particle dispersion (decrease in particle/agglomerate size), led to a decrease in

dielectric constant [67]. Similar findings have been reported for BTO/epoxy composites [68]. Therefore, an improved dispersion, thus an increased interface area between particles and the matrix, decreases the dielectric constant of the composites.

Furthermore, the emergence of a thin interface region between functionalized BTONP and the matrix could also slightly decrease the dielectric properties [69,70]. Particle functionalization leads to strong chemical bonds between the particles and the matrix, which restricts molecular chain movement of the matrix. The literature suggests that the dielectric properties in the transition region can be even smaller for the composite than those of the polymer itself [69], therefore slightly reducing the dielectric constant.

Similar results of a decrease in relative permittivity of the composite materials with functionalized particles were reported by Ramajo [63], where an epoxy duromer was used as a matrix and a methoxysilane (glycidoxy methoxysilane Z-6040 (Dow Corning)) was used as a functionalization agent. The reduction in the dielectric properties of samples with functionalized particles occurred only at high functionalization levels. We think, however, that our results are not comparable because of very different matrix chemistry. In contrast, other literature reports an increase in relative permittivity via binding of (γ-aminopropyl)trimethoxysilane on the particle surface [61], but in this case, non-functionalized nanoparticles already showed good dispersion and, hence, no change in the dispersion state occurred. Another study also showed an increase in dielectric properties when using functionalized BTO [36], but again, a different functionalization agent (γ-aminopropyl)trimethoxysilane (γ-APS)) with a different side group than TMSPM was used.

Decreased dielectric losses because of particle functionalization are desired for piezoelectric composites. This decrease in dielectric loss is caused by improved dispersion of the functionalized BTONP. In general, the increase in secondary particle size (particle agglomeration) leads to higher dissipation factors. This follows the findings of Zhang et al. [67] and other literature [61]. Zhang et al. attributed this behavior to an increase in conduction loss due to a looser structure in agglomerates. It is possible that this can be related to the poor particle-matrix interaction of the particles (gaps between particles and polymer), thus increasing the dissipation factor.

To summarize, a decrease in particle size, due to smaller/fewer agglomerates after functionalization, leads to a decrease in the dielectric constant, while the improved interface interaction of functionalized particles to the matrix leads to a more rigid structure, which in turn results in decreased dielectric losses.

4. Conclusions

A study on the functionalization of barium titanate nanoparticles (BTONP) with TMSPM was conducted, investigating the influence of processing parameters and different solvents/catalysts on the functionalization degree to find the most promising parameters. The resulting BTONP, functionalized with TMSPM, were used to prepare UV light curable suspensions containing 10 vol.% of functionalized nanoparticles in the photopolymer resin. The influence of particle functionalization on the particle dispersion quality, viscosity, curing depth, and dielectric properties were investigated.

The investigation of the functionalization process revealed that a monolayer surface coverage was obtained for added TMSPM amounts larger than 50 wt.% relative to the BTONP. To this end, an elevated process temperature and a reaction time of 24 h were decisive to achieve a maximum grafting density of 1.5 molecules $_{TMSPM}/nm^2$ in a monolayer arrangement. In contrast, the acid-catalyzed method using HCl in an ethanol/water mixture yielded an apparent grafting density of 5.2 molecules $_{TMSPM}/nm^2$ on the BTONP surface in a multilayer arrangement. Glacial acetic acid was proven to not catalyze the reaction sufficiently.

SEM cross-sectional images of the prepared composites with functionalized BTONP showed an improved particle distribution inside the photopolymer resin after particle functionalization, where the dispersion quality improved with the functionalization degree.

Furthermore, particle-matrix adhesion seemed to be highly improved by functionalization. Other measurements showed slightly increased viscosities of the suspensions at low shear rates, reduced dielectric constants, reduced dielectric losses, and reduced curing depths of the samples with functionalized particles, as a result of improved particle dispersion. While homogeneous particle dispersion is of the highest priority to ensure good product quality, an increase in viscosity and reduction of the curing depth negatively affects composite manufacturability and limits higher ceramic loadings. In summary, particle functionalization is a very promising method to achieve homogeneous particle dispersion and improved particle-matrix interface, but needs to be well understood and tailored to ensure optimum results.

Supplementary Materials: The following supporting information can be downloaded at: https://www.mdpi.com/article/10.3390/jcs7020047/s1, Figure S1: SEM image of BTONP, Figure S2: DLS measurement of BTONP in ethanol before and after functionalization, Figure S3: Unnormalized TGA-thermograms of plain and TMSP-functionalized BTONP, Figure S4: FTIR-spectra of TMSPM-modified BTONP at different reaction temperatures, Figure S5: FTIR-spectra of TMSPM-modified BTONP at different time intervals, Figure S6: SEM images of composite microstructures at x50.000, Figure S7: SEM images of composite microstructures at x20.000.

Author Contributions: Conceptualization, software, validation, formal analysis, investigation, writing—original draft preparation, methodology, data curation—A.Z., R.M. and A.M.; validation, visualization—A.Z., R.M., A.M. and V.M.; supervision, project administration—A.Z. and R.M.; funding acquisition, resources—M.S. and G.G.; writing—review and editing—A.Z., R.M., V.M., G.G. and M.S. All authors have read and agreed to the published version of the manuscript.

Funding: This research was funded by the German Research Foundation (Deutsche Forschungsgemeinschaft, DFG), grant number 389409970.

Acknowledgments: We acknowledge support by the Open Access Publication Funds of Technische Universität Braunschweig. The authors are grateful to Bogdan Semenenko for the SEM images.

Conflicts of Interest: The authors declare no conflict of interest. The funders had no role in the design of the study; in the collection, analyses, or interpretation of data; in the writing of the manuscript, or in the decision to publish the results.

References

1. Wilson, J.S. (Ed.) *Sensor Technology Handbook*; Newnes: Amsterdam, The Netherlands, 2005.
2. Wang, Z.; Narita, F. Corona Poling Conditions for Barium Titanate/Epoxy Composites and their Unsteady Wind Energy Harvesting Potential. *Adv. Eng. Mater.* **2019**, *21*, 1900169. [CrossRef]
3. Wang, Z.; Abe, S.; Narita, F. On the Energy Harvesting Potential of Lead-Free Piezoelectric Composites from Air-Flow and Temperature Change. *Res. Dev. Mater. Sci.* **2018**, *5*, 000607. [CrossRef]
4. Sinapius, J.M. *Adaptronics—Smart Structures and Materials*; Springer: Berlin/Heidelberg, Germany, 2021.
5. Giurgiutiu, V. Piezoelectric Wafer Active Sensors. In *Structural Health Monitoring of Aerospace Composites*; Elsevier: Amsterdam, The Netherlands, 2016; pp. 177–248.
6. Malhotra, J.; Patil, S.; Kaur, W.G.; Kumar, V. Energy Harvesting Applications using Piezoelectric Sensors. In Proceedings of the International Conference on Recent Advances in Computational Techniques (IC-RACT), Navi Mumbai, India, 27–28 March 2020. [CrossRef]
7. Shrout, T.R.; Zhang, S.J. Lead-free piezoelectric ceramics: Alternatives for PZT? *J. Electroceramics* **2007**, *19*, 111–124. [CrossRef]
8. Mitkus, R.; Taleb Alashkar, A.; Sinapius, M. An Attempt to Topology Optimize 3D Printed Piezoelectric Composite Sensors for Highest D31 Output. In *ASME 2021 Conference on Smart Materials, Adaptive Structures and Intelligent Systems*; American Society of Mechanical Engineers: New York, NY, USA, 2021; p. 09142021.
9. Roloff, T.; Mitkus, R.; Lion, J.N.; Sinapius, M. (Eds.) *3D Printable Piezoelectric Composite Sensors for Guided Ultrasonic Wave Detection*; MDPI: Basel, Switzerland, 2021.
10. Lin, J.; Chen, G.; Yang, W.; Li, H.; Lei, Q. New potassium sodium niobate/poly(vinylidene fluoride) functional composite films with high dielectric permittivity. *J. Polym. Res.* **2016**, *23*, 152. [CrossRef]
11. Bodkhe, S.; Ermanni, P. Challenges in 3D printing of piezoelectric materials. *Multifunct. Mater.* **2019**, *2*, 22001. [CrossRef]
12. Tiller, B.; Reid, A.; Zhu, B.; Guerreiro, J.; Domingo-Roca, R.; Jackson, J.C.; Windmill, J.F.C. Piezoelectric microphone via a digital light processing 3D printing process. *Mater. Des.* **2019**, *165*, 107593. [CrossRef]

13. Kim, K.; Middlebrook, J.L.; Chen, J.E.; Zhu, W.; Chen, S.; Sirbuly, D.J. Tunable Surface and Matrix Chemistries in Optically Printed (0–3) Piezoelectric Nanocomposites. *ACS Appl. Mater. Interfaces* **2016**, *8*, 33394–33398. [CrossRef]
14. Yang, Y.; Chen, Z.; Song, X.; Zhu, B.; Hsiai, T.; Wu, P.-I.; Xiong, R.; Shi, J.; Chen, Y.; Zhou, Q.; et al. Three dimensional printing of high dielectric capacitor using projection based stereolithography method. *Nano Energy* **2016**, *22*, 414–421. [CrossRef]
15. Kim, K.; Zhu, W.; Qu, X.; Aaronson, C.; McCall, W.R.; Chen, S.; Sirbuly, D.J. 3D optical printing of piezoelectric nanoparticle-polymer composite materials. *ACS Nano* **2014**, *8*, 9799–9806. [CrossRef]
16. Popielarz, R.; Chiang, C.K.; Nozaki, R.; Obrzut, J. Dielectric Properties of Polymer/Ferroelectric Ceramic Composites from 100 Hz to 10 GHz. *Macromolecules* **2001**, *34*, 5910–5915. [CrossRef]
17. Jang, J.H.; Wang, S.; Pilgrim, S.M.; Schulze, W.A. Preparation and Characterization of Barium Titanate Suspensions for Stereolithography. *J. Am. Ceram. Soc.* **2000**, *83*, 1804–1806. [CrossRef]
18. Cui, H.; Hensleigh, R.; Yao, D.; Maurya, D.; Kumar, P.; Kang, M.G.; Priya, S.; Zheng, X. Three-dimensional printing of piezoelectric materials with designed anisotropy and directional response. *Nat. Mater.* **2019**, *18*, 234–241. [CrossRef] [PubMed]
19. Yao, D.; Cui, H.; Hensleigh, R.; Smith, P.; Alford, S.; Bernero, D.; Bush, S.; Mann, K.; Wu, H.F.; Chin-Nieh, M.; et al. Achieving the Upper Bound of Piezoelectric Response in Tunable, Wearable 3D Printed Nanocomposites. *Adv. Funct. Mater.* **2019**, *29*, 1903866. [CrossRef]
20. Mitkus, R.; Pierou, A.; Feder, J.; Sinapius, M. Investigation and Attempt to 3D Print Piezoelectric 0-3 Composites Made of Photopolymer Resins and PZT. In *ASME 2020 Conference on Smart Materials, Adaptive Structures and Intelligent Systems*; American Society of Mechanical Engineers: New York, NY, USA, 2020; p. 09152020.
21. Schmidt, D. Modenselektive Übertragung von Lambwellen in Faserverbundstrukturen. Ph.D. Thesis, Deutsches Zentrum für Luft-und Raumfahrt eV, Braunschweig, Germany, 2014.
22. Griffith, M.L.; Halloran, J.W. Freeform Fabrication of Ceramics via Stereolithography. *J. Am. Ceram. Soc.* **1996**, *79*, 2601–2608. [CrossRef]
23. Badev, A.; Abouliatim, Y.; Chartier, T.; Lecamp, L.; Lebaudy, P.; Chaput, C.; Delage, C. Photopolymerization kinetics of a polyether acrylate in the presence of ceramic fillers used in stereolithography. *J. Photochem. Photobiol. A Chem.* **2011**, *222*, 117–122. [CrossRef]
24. Sun, C.; Zhang, X. Experimental and numerical investigations on microstereolithography of ceramics. *J. Appl. Phys.* **2002**, *92*, 4796–4802. [CrossRef]
25. Sun, C.; Zhang, X. The influences of the material properties on ceramic micro-stereolithography. *Sens. Actuators A Phys.* **2002**, *101*, 364–370. [CrossRef]
26. Zhang, X.; Jiang, X.; Sun, C. Micro-stereolithography of polymeric and ceramic microstructures. *Sens. Actuators A Phys.* **1999**, *77*, 149–156. [CrossRef]
27. Liu, J.; Tian, G.; Qi, S.; Wu, Z.; Wu, D. Enhanced dielectric permittivity of a flexible three-phase polyimide–graphene–BaTiO3 composite material. *Mater. Lett.* **2014**, *124*, 117–119. [CrossRef]
28. Luo, C.; Hu, S.; Xia, M.; Li, P.; Hu, J.; Li, G.; Jiang, H.; Zhang, W. A Flexible Lead-Free $BaTiO_3$ /PDMS/C Composite Nanogenerator as a Piezoelectric Energy Harvester. *Energy Technol.* **2018**, *6*, 922–927. [CrossRef]
29. Zhang, Y. In Situ Fatigue Crack Detection using Piezoelectric Paint Sensor. *J. Intell. Mater. Syst. Struct.* **2016**, *17*, 843–852. [CrossRef]
30. Escamilla-Díaz, T.; Serralta-Macías, J.J.; García-Zaldivar, O.; Cruz-Valeriano, E.; Ramírez-Bon, R.; Yanez Limon, J.M. Optical and dielectric studies of PMMA: Precursors of BNT hybrid films. *Appl. Phys. A* **2019**, *125*, 376. [CrossRef]
31. Gupta, S.; Bhunia, R.; Fatma, B.; Maurya, D.; Singh, D.; Gupta, R.; Priya, S.; Gupta, R.K.; Gang, A. Multifunctional and Flexible Polymeric Nanocomposite Films with Improved Ferroelectric and Piezoelectric Properties for Energy Generation Devices. *ACS Appl. Energy Mater.* **2019**, *2*, 6364–6374. [CrossRef]
32. Zarinwall, A.; Waniek, T.; Saadat, R.; Braun, U.; Sturm, H.; Garnweitner, G. Comprehensive Characterization of APTES Surface Modifications of Hydrous Boehmite Nanoparticles. *Langmuir* **2021**, *37*, 171–179. [CrossRef]
33. Zarinwall, A.; Waniek, T.; Finke, B.; Saadat, R.; Sturm, H.; Garnweitner, G. Particle Surface Modification. In *Acting Principles of Nano-Scaled Matrix Additives for Composite Structures*; Sinapius, M., Ziegmann, G., Eds.; Springer: Cham, Switzerland, 2021; pp. 119–142.
34. Mitkus, R.; Scharnofske, M.; Sinapius, M. Characterization 0.1 wt.% Nanomaterial/Photopolymer Composites with Poor Nanomaterial Dispersion: Viscosity, Cure Depth and Dielectric Properties. *Polymers* **2021**, *13*, 3948. [CrossRef]
35. Mitkus, R.; Sinapius, M. Piezoelectric Ceramic/Photopolymer Composites Curable with UV Light: Viscosity, Curing Depth, and Dielectric Properties. *J. Compos. Sci.* **2022**, *6*, 212. [CrossRef]
36. Phan TT, M.; Chu, N.C.; van Luu, B.; Nguyen Xuan, H.; Pham, D.T.; Martin, I.; Carriere, P. Enhancement of polarization property of silane-modified $BaTiO_3$ nanoparticles and its effect in increasing dielectric property of epoxy/$BaTiO_3$ nanocomposites. *J. Sci. Adv. Mater. Devices* **2016**, *1*, 90–97. [CrossRef]
37. Hasbullah, N.N.; Lee, O.J.; Chyi JL, Y.; Chen, S.K.; Talib, Z.A. Synthesis of $BaTiO_3$ Nanoparticles via Hydrothermal Method. *Solid State Phenom.* **2017**, *268*, 172–176. [CrossRef]
38. Liu, Y.; Li, Y.; Li, X.-M.; He, T. Kinetics of (3-aminopropyl)triethoxylsilane (APTES) silanization of superparamagnetic iron oxide nanoparticles. *Langmuir* **2013**, *29*, 15275–15282. [CrossRef]
39. Lee, T.-J.; Chau, L.-K.; Huang, C.-J. Controlled Silanization: High Molecular Regularity of Functional Thiol Groups on Siloxane Coatings. *Langmuir* **2020**, *36*, 5935–5943. [CrossRef]

40. Rozlosnik, N.; Gerstenberg, M.C.; Larsen, N.B. Effect of Solvents and Concentration on the Formation of a Self-Assembled Monolayer of Octadecylsiloxane on Silicon (001). *Langmuir* **2003**, *19*, 1182–1188. [CrossRef]
41. Zarinwall, A.; Asadian-Birjand, M.; Seleci, D.A.; Maurer, V.; Trautner, A.; Garnweitner, G.; Fuchs, H. Magnetic Nanoparticle-Based Dianthin Targeting for Controlled Drug Release Using the Endosomal Escape Enhancer SO1861. *Nanomaterials* **2021**, *11*, 1057. [CrossRef] [PubMed]
42. Zarinwall, A.; Maurer, V.; Pierick, J.; Oldhues, V.M.; Porsiel, J.C.; Finke, J.H.; Garnweitner, G. Amorphization and modified release of ibuprofen by post-synthetic and solvent-free loading into tailored silica aerogels. *Drug Deliv.* **2022**, *29*, 2086–2099. [CrossRef] [PubMed]
43. Galeotti, F.; Bertini, F.; Scavia, G.; Bolognesi, A. A controlled approach to iron oxide nanoparticles functionalization for magnetic polymer brushes. *J. Colloid Interface Sci.* **2011**, *360*, 540–547. [CrossRef] [PubMed]
44. Vrancken, K.C.; van der Voort, P.; Possemiers, K.; Vansant, E.F. Surface and Structural Properties of Silica Gel in the Modification with γ-Aminopropyltriethoxysilane. *J. Colloid Interface Sci.* **1995**, *174*, 86–91. [CrossRef]
45. Čampelj, S.; Makovec, D.; Drofenik, M. Functionalization of magnetic nanoparticles with 3-aminopropyl silane. *J. Magn. Magn. Mater.* **2009**, *321*, 1346–1350. [CrossRef]
46. Kaur, J.; Kotnala, R.K.; Verma, K.C. Surfactant free hydrothermal synthesis, electrical, optical and ferroelectric properties of BaTiO3 nanoparticles. *J. Optoelectron. Adv. Mater.* **2012**, *14*, 219–223.
47. Singh, M.; Yadav, B.C.; Ranjan, A.; Kaur, M.; Gupta, S.K. Synthesis and characterization of perovskite barium titanate thin film and its application as LPG sensor. *Sens. Actuators B Chem.* **2017**, *241*, 1170–1178. [CrossRef]
48. Ashiri, R. Detailed FT-IR spectroscopy characterization and thermal analysis of synthesis of barium titanate nanoscale particles through a newly developed process. *Vib. Spectrosc.* **2013**, *66*, 24–29. [CrossRef]
49. Haroon, A.; Rai, P.; Uddin, I. Synthesis, Characterization and Dielectric Properties of $BaTiO_3$ Nanoparticles. *Int. J. Nanosci.* **2020**, *19*, 1950001. [CrossRef]
50. Bressy, C.; van Ngo, G.; Ziarelli, F.; Margaillan, A. New insights into the adsorption of 3-(trimethoxysilyl)propylmethacrylate on hydroxylated ZnO nanopowders. *Langmuir* **2012**, *28*, 3290–3297. [CrossRef] [PubMed]
51. Arantes, T.M.; Pinto, A.H.; Leite, E.R.; Longo, E.; Camargo, E.R. Synthesis and optimization of colloidal silica nanoparticles and their functionalization with methacrylic acid. *Colloids Surf. A Physicochem. Eng. Asp.* **2012**, *415*, 209–217. [CrossRef]
52. Nazir, T.; Afzal, A.; Siddiqi, H.M.; Saeed, S.; Dumon, M. The influence of temperature and interface strength on the microstructure and performance of sol–gel silica–epoxy nanocomposites. *Polym. Bull.* **2011**, *67*, 1539–1551. [CrossRef]
53. Pasternack, R.M.; Rivillon Amy, S.; Chabal, Y.J. Attachment of 3-(Aminopropyl)triethoxysilane on silicon oxide surfaces: Dependence on solution temperature. *Langmuir* **2008**, *24*, 12963–12971. [CrossRef]
54. Etienne, M. Analytical investigation of the chemical reactivity and stability of aminopropyl-grafted silica in aqueous medium. *Talanta* **2003**, *59*, 1173–1188. [CrossRef]
55. Vansant, E.F.; van der Voort, P.; Vrancken, K.C. *Characterization and Chemical Modification of the Silica Surface*; Elsevier: Amsterdam, The Netherlands, 1995; p. 556.
56. Fadeev, A.Y.; Helmy, R.; Marcinko, S. Self-Assembled Monolayers of Organosilicon Hydrides Supported on Titanium, Zirconium, and Hafnium Dioxides. *Langmuir* **2002**, *18*, 7521–7529. [CrossRef]
57. Osterholtz, F.D.; Pohl, E.R. Kinetics of the hydrolysis and condensation of organofunctional alkoxysilanes: A review. *J. Adhes. Sci. Technol.* **1992**, *6*, 127–149. [CrossRef]
58. Pantoja, M.; Velasco, F.; Broekema, D.; Abenojar, J.; Del Real, J.C. The Influence of pH on the Hydrolysis Process of γ-Methacryloxypropyltrimethoxysilane, Analyzed by FT-IR, and the Silanization of Electrogalvanized Steel. *J. Adhes. Sci. Technol.* **2010**, *24*, 1131–1143. [CrossRef]
59. Serjeant, E.P.; Dempsey, B. *Ionisation Constants of Organic Acids in Aqueous Solution*; Pergamon Pr: Oxford, UK, 1979; p. 989.
60. Riedel, E. *Anorganische Chemie*, 6th ed.; de Gruyter: Berlin, Germany, 2004; p. 935.
61. Dang, Z.-M.; Yu, Y.-F.; Xu, H.-P.; Bai, J. Study on microstructure and dielectric property of the BaTiO3/epoxy resin composites. *Compos. Sci. Technol.* **2008**, *68*, 171–177. [CrossRef]
62. Andrew, W. *Ceramic Thick Films for MEMS and Microdevices*; William Andrew: Oxford, UK, 2011.
63. Ramajo, L.; Castro, M.S.; Reboredo, M.M. Effect of silane as coupling agent on the dielectric properties of $BaTiO_3$-epoxy composites. *Compos. Part A Appl. Sci. Manuf.* **2007**, *38*, 1852–1859. [CrossRef]
64. Zhang, X.; Ma, Y.; Zhao, C.; Yang, W. High dielectric constant and low dielectric loss hybrid nanocomposites fabricated with ferroelectric polymer matrix and $BaTiO_3$ nanofibers modified with perfluoroalkylsilane. *Appl. Surf. Sci.* **2014**, *305*, 531–538. [CrossRef]
65. Bareiro Ferreira, O.; Sridaran Venkat, R.; Adam, J.; Boller, C. Development of the Fabrication Process and Characterization of Piezoelectric $BaTiO_3$/Epoxy Composite Used for Coated Ultrasonic Transducer Patterns in Structural Health Monitoring. In Proceedings of the 19th World Conference on Non-Destructive Testing, Munich, Germany, 13–17 June 2016.
66. Robertson, J.; Varlow, B.R. Non-linear ferroelectric composite dielectric materials. *IEEE Trans. Dielectr. Electr. Insul.* **2005**, *12*, 779–790. [CrossRef]
67. Zhang, Y.; Liu, Z.; Ding, F.; Zhang, W. Effect of piezoelectric ceramic particles size gradation on piezoelectric properties of 0–3 cement-based piezoelectric composites. *Smart Mater. Struct.* **2018**, *27*, 85029. [CrossRef]

68. Cho, S.-D.; Lee, J.-Y.; Paik, K.-W. Effects of particle size on dielectric constant and leakage current of epoxy/barium titanate ($BaTiO_3$) composite films for embedded capacitors. In *Advances in Electronic Materials and Packaging 2001 (Cat. No.01EX506)*; IEEE: New York, NY, USA, 2001; pp. 63–68.
69. Tan, Q.; Cao, Y.; Irwin, P. DC Breakdown in Polyetherimide Composites and Implication for Structural Engineering. In Proceedings of the 2007 IEEE International Conference on Solid Dielectrics, Winchester, UK, 8–13 July 2007; IEEE: New York, NY, USA, 2007; pp. 411–414.
70. Wang, W. Li, S. A transition of interface characteristics in LDPE/Al2O3 nanocomposites by permittivity simulation. In *IEEE Transactions on Dielectrics and Electrical Insulation*; IEEE: New York, NY, USA, 2018; Volume 25, pp. 2–12. [CrossRef]